



Alternative approaches used to assess structural changes of natural zircon caused by heat treatment

L.T.T. Huong^{a,*}, N.T.M. Thuyet^a, T.L. Phan^{b,*}, N. Tran^b, D.N. Toan^c, P.D. Thang^d, B.T. Huy^e

^a Faculty of Geology, University of Science, Vietnam National University, 334 Nguyen Trai, Hanoi, Vietnam

^b Department of Physics and Oxide Research Center, Hankuk University of Foreign Studies, Yongin 449-791, South Korea

^c Institute of Research and Development, Duy Tan University, Da Nang, Vietnam

^d Faculty of Engineering Physics and Nanotechnology, VNU – University of Engineering and Technology, Xuan Thuy, Cau Giay, Hanoi, Vietnam

^e Department of Chemistry, Changwon National University, Changwon 641-773, South Korea

ARTICLE INFO

Keywords:

Zircon
Heat treatment
Crystal structure
Optical and magnetic properties

ABSTRACT

It is known that large changes in the crystal structure of zircon (ZrSiO_4) can be assessed through the linewidth of the characteristic Raman mode ($\Delta\nu_3$) at 1008 cm^{-1} . However, the use of $\Delta\nu_3$ to assess small changes caused by heat treatment at temperatures below its decomposition temperature of $\sim 1670\text{ }^\circ\text{C}$ is difficult. The present work points out that the combination of X-ray diffraction (XRD) analyses, and photoluminescence (PL) and Raman (RS) measurements with different excitation wavelengths is an effective approach to solve the above problem. In this context, we have selected natural zircon containing some rare-earth (RE) impurities, and then studied the changes in its crystal structure caused by heat treatment at temperatures $T_{\text{an}}=400\text{--}1600\text{ }^\circ\text{C}$. XRD analyses reveal that small modifications of the unit-cell parameters occur as $T_{\text{an}} > 600\text{ }^\circ\text{C}$. Taking the intensity ratios of the ν_3 mode to RE-related emissions (I_{ν_3}/I_{RE}) or the PL intensity ratios between RE-related emissions into consideration, the similar results in good agreement with the XRD analyses are also found. We believe that the small structural changes are related to the migration and redistribution of defects and impurities, and re-crystallization of zircon. This could be further confirmed though the relation between paramagnetic and ferromagnetic signals when T_{an} changes.

1. Introduction

Zirconium silicate occurs in nature as zircon with the chemical formula of ZrSiO_4 , where Zr is partially substituted by Hf (1–4 wt%) and actinides of U and Th [1]. Depending on geographical location, a large variety of transition and rare-earth (RE) metal cations with very small amounts can also be present in zircon [2]. The existence of U and Th causes radioactive decay and various structure transformations (such as the loss of translational symmetry, generation of point defects, formation of metastable phases, and metamictization) [3–5]. Particularly, due to the structural resilience versus high radiation doses over significant time-scales, zircon has been suggested as a promising material for age dating of igneous rocks, and a long-term storage of nuclear wastes [3,4,6]. Apart from these behaviors, zircon has been proven to be a hard material, with hardness ranging from 6.5 to 7.5. With low-thermal expansion and conductivity, high resistance to thermal shock, good corrosion resistance, and highly chemical stability, it is also widely used in the ceramic, foundry, and refractory industries [2,7,8].

Previous studies pointed out that the crystal structure of natural ZrSiO_4 is very stable versus thermal processes up to about $1700\text{ }^\circ\text{C}$ [1,9]. While large structural changes usually caused by high irradiation doses, geological processes, or applied high pressures can be assessed effectively through the linewidth of the characteristic Raman mode ($\Delta\nu_3$) at 1008 cm^{-1} [5,10], the assessment of small structural changes induced by heat treatment at temperatures below zircon's decomposition temperature of $\sim 1670\text{ }^\circ\text{C}$ based on $\Delta\nu_3$ is impossible. The seeking of other suitable approaches is thus necessary to solve this issue. Additionally, it comes to our attention that the correlation between the crystal structure and the optical and magnetic properties versus heat treatment of zircon was not taken into account.

This work bases on sensitive probes of X-ray diffraction (XRD), photoluminescence (PL) and Raman spectroscopy, and vibrating sample magnetometer to solve the above problems. The XRD analyses indicate that small modifications of the unit-cell parameters occur as $T_{\text{an}} > 600\text{ }^\circ\text{C}$. Taking into account for the intensity ratios of the ν_3 mode to RE-related emissions (I_{ν_3}/I_{RE}), or the PL intensity ratios between RE-related emissions, the results in good agreement with the XRD

* Corresponding authors.

E-mail addresses: ltthuongvnu@yahoo.com (L.T.T. Huong), ptlong2512@yahoo.com (T.L. Phan).

<http://dx.doi.org/10.1016/j.physb.2017.03.007>

Received 7 December 2016; Received in revised form 1 March 2017; Accepted 2 March 2017
0921-4526/ © 2017 Elsevier B.V. All rights reserved.

analyses are also found. We think that the small structural changes caused by heat treatment are due to the migration and redistribution of defects and impurities, and/or re-crystallization. This would be additionally confirmed though the relation between the paramagnetic (PM) and ferromagnetic (FM) behaviors.

2. Experimental details

A natural zircon fragment with uniform reddish-brown color collected from a mine in Central Highlands of Vietnam was used for this study. The as-received sample was then cut into small pieces. One part was polished its surface for analyzing chemical components based on electron micro-probe analyses (EMPA), using a JEOL JXA-8900RL microscope equipped with wavelength dispersive spectroscopy, and on a laser ablation-inductively coupled plasma-mass spectrometry (LA-ICPMS). Results of chemical-composition analysis revealed a fairly homogeneous distribution of elements in zircon, which is constituted of ZrO_2 (65.811 wt%), SiO_2 (32.342 wt%) and HfO_2 (1.08 wt%). Other elements such as Th (84.54 ppm) and U (100.9 ppm), Nd (0.64 ppm), Dy (33.78 ppm), Er (55.31 ppm), Tm (11.57 ppm), and several transition metals were also traced. Remaining zircon parts were used to anneal in air for 12 h at temperatures (T_{an}) in the range 400–1600 °C. After annealing, the crystal structure of final products was checked by an X-ray diffractometer (Rigaku, MiniFlex), working with a $\text{Cu-K}\alpha$ radiation source ($\lambda=1.5406 \text{ \AA}$) and fixed scanning steps of 0.01° . Their PL and Raman scattering (RS) spectra were studied by using Acton-SpectraPro fluorescence (750-Triplet Grating Monochromator) and XPLORA-Plus Horiba micro-Raman spectrometers, which worked with excitation wavelengths (λ_{exc}) of 355, 532, and 785 nm. Magnetization versus magnetic-field measurements were performed on a vibrating sample magnetometer (VSM, LakeShore 736). All measurements were carried out at room temperature.

3. Results and discussion

Concerning heat treatment, we found that natural color of zircon (reddish brown) is paled soon after annealing at 400 °C. Particularly, it becomes colorless as $T_{\text{an}}=1600 \text{ °C}$. The crystal structure of these samples was then checked by an X-ray diffractometer. Fig. 1(a) shows an XRD pattern of the unheated sample in the angle range $20^\circ \leq 2\theta \leq 70^\circ$. The results of structural analyses based on the Rietveld technique (used the FullProf Suite program) reveal the best fit between the experimental and calculated patterns (with $\chi^2 \approx 4\%$), and this sample to be single phase in a tetragonal structure (the $I41/amd$ space group), with the lattice constants $a=b=6.6045(3) \text{ \AA}$ and $c=5.9783(3) \text{ \AA}$, and the unit-cell volume $V=260.769(9) \text{ \AA}^3$. Fitting the experimental data is also shown in Fig. 1(a). The coordinates of Zr, Si and O atoms, inter-atomic lengths and bond angles obtained from the refinement are listed in Table 1. For the structure of zircon, it consists of chains of $[\text{SiO}_4]$ tetrahedra and $[\text{ZrO}_6]$ polyhedra, Fig. 1(b). There are one Si-O bond length ($\times 4$) $1.624(1) \text{ \AA}$, and two independent Zr-O bonds ($\times 4$) of lengths $2.116(4) \text{ \AA}$ and $2.270(2) \text{ \AA}$. For $[\text{SiO}_4]$ tetrahedra, there are two different bond angles with $\text{O-Si-O}(1)=115.93(6)^\circ$ and $\text{O-Si-O}(2)=97.20(6)^\circ$. Small differences among refinement results are usually ascribed to minor metamictization existing in natural zircons and/or problems related to extinction [4]. Notably, an accurate identification of the Hf site in ZrSiO_4 based on Rietveld refinement for normal XRD patterns is impossible because of very mirror structural and electronic differences between Zr and Hf.

In Fig. 2, it shows the XRD patterns of the heated samples. The feature of the patterns is quite the same as that of the unheated sample, consisting of the sharp and strong-intensity peaks from tetragonal ZrSiO_4 . Having performed the Rietveld refinement for these data (within $\chi^2=4\text{--}6\%$), we determined the values of the unit-cell parameters a , c , and V , as graphed in Fig. 3. Their changes at temperatures $T_{\text{an}} > 600 \text{ °C}$ are very small (about 0.1–0.2%), which are ascribed to the

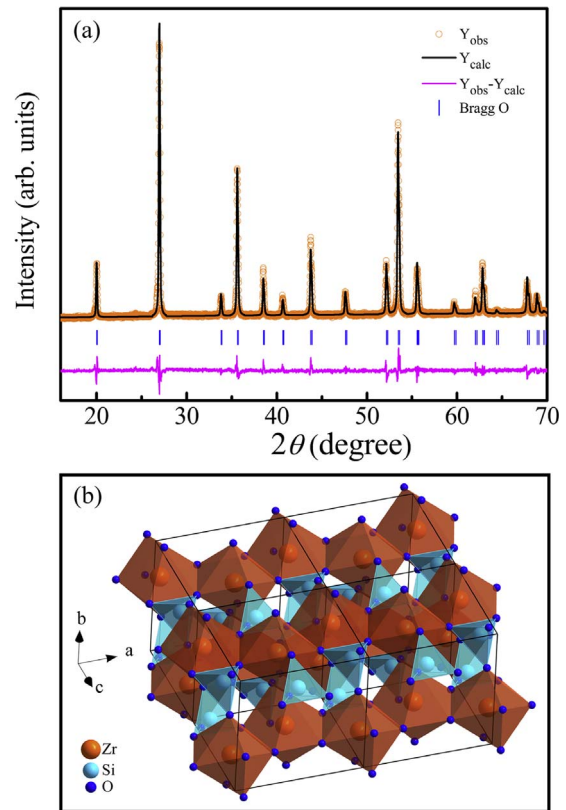


Fig. 1. (a) XRD pattern and Rietveld refinement (carried out for the $I41/amd$ structure) for the unheated sample, where Y_{obs} and Y_{calc} are the Bragg peak positions of the observed and calculated patterns, respectively, and the difference between Y_{obs} and Y_{calc} data ($Y_{\text{obs}}-Y_{\text{calc}}$) is shown at the bottom. (b) The crystal structure of ZrSiO_4 is formed from the chains of alternating edge-sharing $[\text{ZrO}_6]$ polyhedra and $[\text{SiO}_4]$ tetrahedra.

migration and redistribution of defects and impurities, and/or the re-crystallization of aperiodic/amorphous state (this state is generated from metamictization) when natural zircon is subjected to the annealing. The results indicate that the crystal structure of zircon is very stable, even at high temperatures up to 1600 °C. This is understandable because the dissociation of ZrSiO_4 usually takes place above 1670 °C [1,9].

In addition to the structural check based on XRD, we have studied the RS spectra of the samples. The feature of phonon-vibration modes can give more information about local structures of zircons. For this purpose, we recorded RS spectra at different positions on the samples. The data obtained from these positions were averaged to release the final data. As mentioned above that zircon belongs to the $I41/amd$ space group, its vibration spectrum thus consists of 36 modes, occurring with $\Gamma=2A_{1g}+4B_{1g}+5E_g+A_{2g}+B_{1u}+A_{1u}+2B_{2u}+4A_{2u}+5E_u$ [11]. Among these, the first four terms ($2A_{1g}+4B_{1g}+B_{2g}+5E_g$) characterize 12 Raman-active modes, and the A_{2u} and E_u modes are active in the infrared (i.e., acoustic and IR-activated modes) [1,4,5]. Its has

Table 1

The atomic coordinates and isotropic displacement parameters of $I41/amd$ tetragonal ZrSiO_4 (the unheated sample) at room temperature.

Atom	Site	x	y	z
Zr	$4a$	0	3/4	1/8
Si	$4b$	0	3/4	5/8
O	$16h$	0	0.0656(2)	0.1954(3)
Si-O [$\times 4$]			$1.624(1) \text{ \AA}$	$\text{O-Si-O}(1)=115.93(6)^\circ$
Zr-O [$\times 4$]			$2.116(4) \text{ \AA}$	$\text{O-Si-O}(2)=97.20(6)^\circ$
Zr-O [$\times 4$]			$2.270(2) \text{ \AA}$	

* Square-bracketed numbers are bond multiplicities.

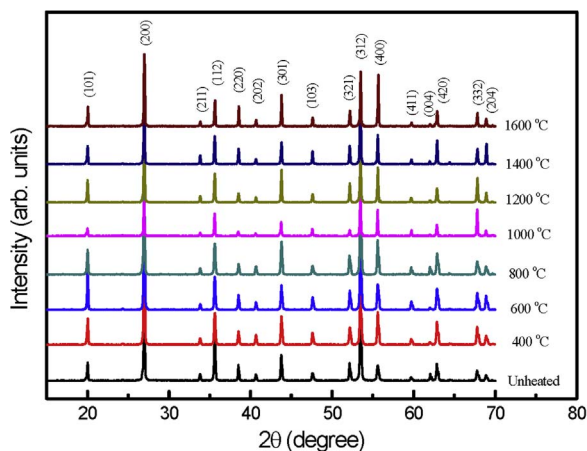


Fig. 2. Miller-indexed XRD patterns of the samples annealed at temperatures $T_{an}=400$ – 1600 °C compared with the XRD pattern the unheated sample.

been suggested that the intensive Raman bands of zircon lying in the wavenumber range 350 – 450 cm^{-1} and around 1000 cm^{-1} are interpreted as internal vibrations of SiO_4 units, and intense external lattice vibrations (rotational and translational) occur in the range of 200 – 230 cm^{-1} [2]. Fully observing these modes is usually based on Raman and IR techniques, particularly the record of polarized Raman spectra [1,4,11]. The change in laser power [3] and pressure [7] also influence strongly the observation and feature of vibration modes. Detailed descriptions and assignments of Raman and IR modes can be found elsewhere [4,7,11]. In this work, we used laser wavelengths $\lambda_{exc.}=785$ and 355 nm to excite vibration modes of the zircon samples. The use of different excitation wavelengths limits unexpected mistakes in addressing RS modes, because RS spectra of natural zircons usually accompany with PL emissions related to electronic transitions of RE ions [12]. Also, the peak position of RS modes is almost unchanged while that of PL emissions is strongly dependent on excitation wavelength. Fig. 4 shows RS spectra in the wavenumber range 120 – 1250 cm^{-1} of the unheated sample. Under the excitation of $\lambda_{exc.}=785$ nm, the RS spectrum indicates many peaks coming from both RS modes and PL-related RE emissions. Among these, the broad band combined with some dominant large-width peaks at wavenumbers of 250 – 700 cm^{-1} (i.e., 800 – 830 nm) are due to the $^3\text{H}_4 \rightarrow ^3\text{H}_6$ transition of Tm^{3+} , and a set of peaks at wavenumbers 1200 – 1600 cm^{-1} (865 – 900 nm) is associated with the $^4\text{F}_{3/2} \rightarrow ^4\text{I}_{9/2}$ transition of Nd^{3+} [12]. The nature of remain narrow peaks can be identified if comparing with the RS spectrum recorded for $\lambda_{exc.}=532$ nm, Fig. 4 (the below panel). It

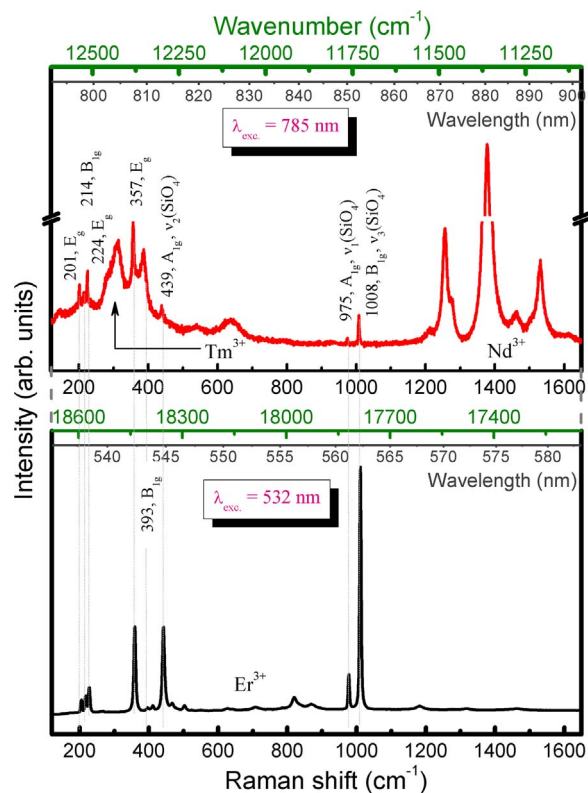


Fig. 4. RS spectra of the unheated red-brown zircon excited by wavelengths of $\lambda_{exc.}=785$ nm (the upper panel) and $\lambda_{exc.}=355$ nm (the below panel).

appears that the positions of narrow peaks at about 201 , 214 , 224 , 357 , 393 , 439 , 775 and 1008 cm^{-1} are independent of excitation wavelengths, the dotted lines in Fig. 4. They are thus proven to be active Raman modes, and associated with the assigned processes E_g (211 , 224 , and 357 cm^{-1}), B_{1g} (214 , 393 , and 1008 cm^{-1}), and A_{1g} (439 and 975 cm^{-1}) [1,4,11]. Besides these RS modes, we also found some PL peaks associated with the $^4\text{S}_{3/2} \rightarrow ^4\text{I}_{15/2}$ transition of Er^{3+} ions [12].

If plotting all the RS spectra of the unheated and heated zircon samples, Figs. 5 and 6, one can figure out how heat treatment influences vibration modes. In general, their spectral shape is quite the same. Similar to the case of the unheated sample, the spectra of the heated samples consist of PL emissions of Tm^{3+} and Nd^{3+} for $\lambda_{exc.}=785$ nm, Er^{3+} for $\lambda_{exc.}=532$ nm, and RS modes. The position of spectral peaks is almost independent of T_{an} . Small differences in the spectral feature can be seen, such as the number of visible peaks and their intensity. If more attention is given to the feature of the spectra shown in Fig. 5, particularly at wavenumbers about 300 and 1000 cm^{-1} , one can see a clear change in the intensity of some peaks. As discussed previously [12], without any internal/external calibrations, the accurate determination of absolute intensities of PL and RS peaks is very difficult. However, the assessment of their relative intensity variations can be visualized. In this context, we have considered the relation between the characteristic vibration mode of zircon at 1008 cm^{-1} (i.e., B_{1g} associated with anti-symmetric stretching of SiO_4 tetrahedra, also denoted as $\nu_3(\text{SiO}_4)$ or ν_3 [4,7]) and one Tm^{3+} -related emission centered at ~ 300 cm^{-1} (~ 805 nm), Fig. 5, corresponding to relative intensities named I_{ν_3} and I_{Tm} , respectively, for $\lambda_{exc.}=785$ nm. Fig. 7(a) plots dependences of the I_{ν_3}/I_{Tm} ratio on T_{an} . It shows that I_{ν_3} tends to decrease if zircon is annealed at temperatures $T_{an}=400$ – 600 °C. With $T_{an} > 600$ °C, an increase in T_{an} enhances quickly I_{ν_3} . If carrying out the same route for the RS spectra with $\lambda_{exc.}=532$ nm, and the relative intensity of an Er^{3+} -related emission at ~ 816 cm^{-1} (~ 556 nm) is denoted as I_{Er} , Fig. 6, the assessment of T_{an} dependences of the I_{ν_3}/I_{Er} ratio also gives a variation tendency similar

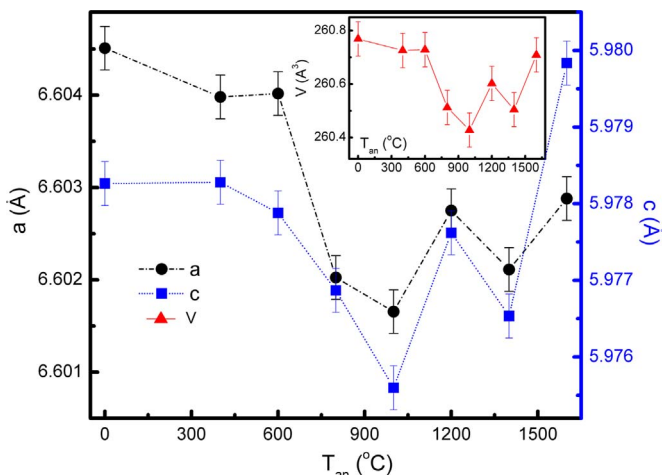


Fig. 3. Variation of the unit-cell parameters of ZrSiO_4 versus the annealing with $T_{an}=400$ – 1600 °C. Error bars of 2% are also shown.

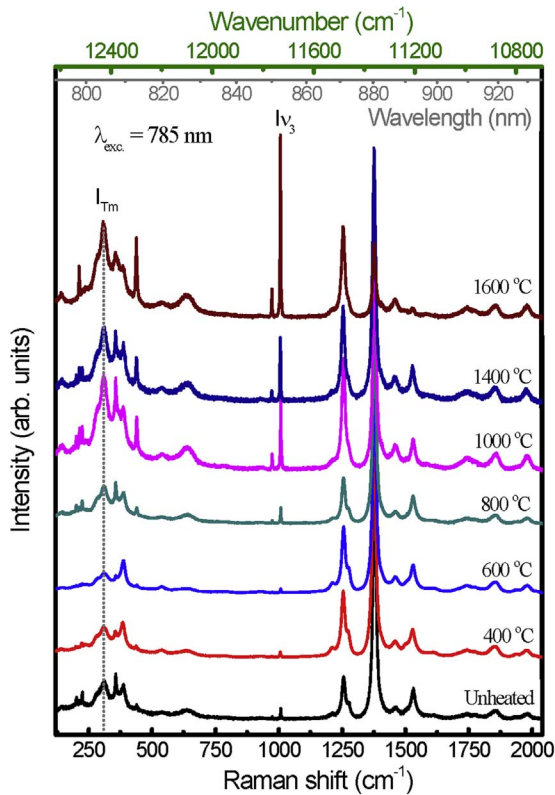


Fig. 5. RS spectra of the unheated and heated samples excited by wavelength $\lambda_{\text{exc}}=785$ nm.

to the I_{v_3}/I_{Tm} case, as shown in the inset of Fig. 7(a). Such the results demonstrate the dependence of the $v_3(\text{SiO}_4)$ intensity I_{v_3} on T_{an} . In the present work, we have also considered the variation of the full width at half maximum of the $v_3(\text{SiO}_4)$ mode (denoted as Δv_3) versus T_{an} . The data shown in Fig. 7(b) reveal a strong dependence of Δv_3 on excitation

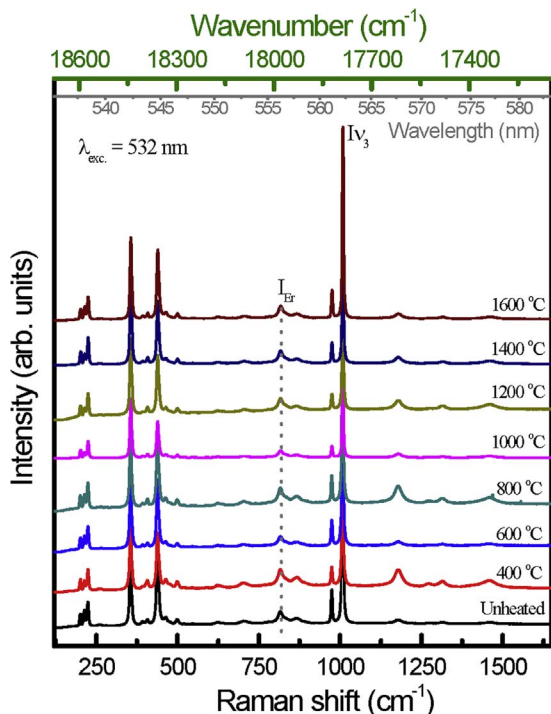


Fig. 6. RS spectra of the unheated and heated samples excited by wavelength $\lambda_{\text{exc}}=532$ nm.

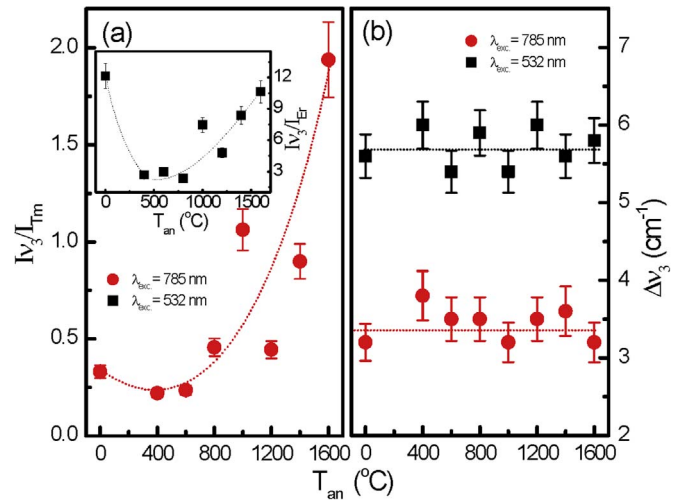


Fig. 7. T_{an} dependences of (a) the I_{v_3}/I_{Tm} ratio and (b) Δv_3 of the samples excited by laser wavelengths $\lambda_{\text{exc}}=785$ and 355 nm. Error bars of 5% are also shown.

wavelength λ_{exc} . This was not taken into account in earlier works [1,3,4,7,10,13]. As a result, Δv_3 values vary in the ranges $3.2\text{--}3.8\text{ cm}^{-1}$ and $5.3\text{--}6\text{ cm}^{-1}$ for $\lambda_{\text{exc}}=785$ and 532 nm, respectively. If using the relation between Δv_3 and α -dose [10], we can estimate α -dose existing in our zircon samples to be $2\text{--}4 \times 10^{17}$ events/g. It should be noticed that with the feature of the Δv_3 data shown in Fig. 7(b), it is difficult to assess the influence of heat treatment on the crystal structure. It has been suggested that the variation of the spectral parameters of $v_3(\text{SiO}_4)$ are proportional to the disorder, defects and damage levels in zircon [2,3,5,7,13]. For our samples, however, the use of the $v_3(\text{SiO}_4)$ -peak position and Δv_3 only is not effective to assess these problems since their change versus T_{an} is unclear. This is probably due to the fact that the annealing mainly influences the distribution, migration and/or disappearance of point defects and impurities. Also, the crystalline fraction could increase due to the crystallization of an aperiodic/amorphous part usually present in mineral zircons. Under such the situation, the unit-cell parameters and the intensities of characteristic Raman modes and PL peaks would be changed. We thus think that the assessment of small structural variations caused by heat treatment at temperatures below the decomposition temperature (~ 1670 °C [1,9]) can be based on the I_{v_3}/I_{Tm} and/or I_{v_3}/I_{Er} ratios. Larger changes (such as large damages and lattice disorders, or decomposition of ZrSiO_4 into ZrO_2 and SiO_2) due to high irradiation doses and geological processes and/or high-temperature annealing (> 1670 °C) would result in larger Δv_3 changes. It is necessary to say additionally that the decrease of I_{v_3}/I_{Tm} and I_{v_3}/I_{Er} (i.e., I_{v_3}) of the heated samples with $T_{\text{an}}=400\text{--}600$ °C compared with the unheated sample is due to the migration and re-distribution of point defects because the unit-cell parameters are almost unchanged in this temperature region, as seen in Fig. 3.

We have also recorded the PL spectra of the samples excited by $\lambda_{\text{exc}}=355$ nm, as shown representatively in Fig. 8, in the wavelength range $400\text{--}680$ nm. For the unheated sample, its spectrum exhibit broad and narrow emissions. Among these, the broad emissions at wavelengths below 460 nm are thought to intrinsic/point defects, such as oxygen defects on bridging oxygens [6], while other groups of narrow peaks at about 480 , 580 , and 665 nm are associated with electronic transitions of ${}^4\text{F}_{9/2} \rightarrow {}^6\text{H}_{15/2}$, ${}^4\text{F}_{9/2} \rightarrow {}^6\text{H}_{13/2}$, and ${}^4\text{F}_{9/2} \rightarrow {}^6\text{H}_{11/2}$, respectively, of Dy^{3+} ions [6,12]. Surprisingly, the annealing from 400 °C to 1600 °C leads to the disappearance of these broad emissions, which could be linked to the color change from reddish brown of zircon to others. Previously, it was found that yellow broad-band luminescence nearly totally disappears when natural zircons were heated at 800 °C, or irradiated by different α -doses [14]. For the heated samples, their spectra only exhibits the Dy^{3+} -related emissions. If denoting $I_{\text{Dy}1}$ and $I_{\text{Dy}2}$ are integrated intensities of the PL emissions

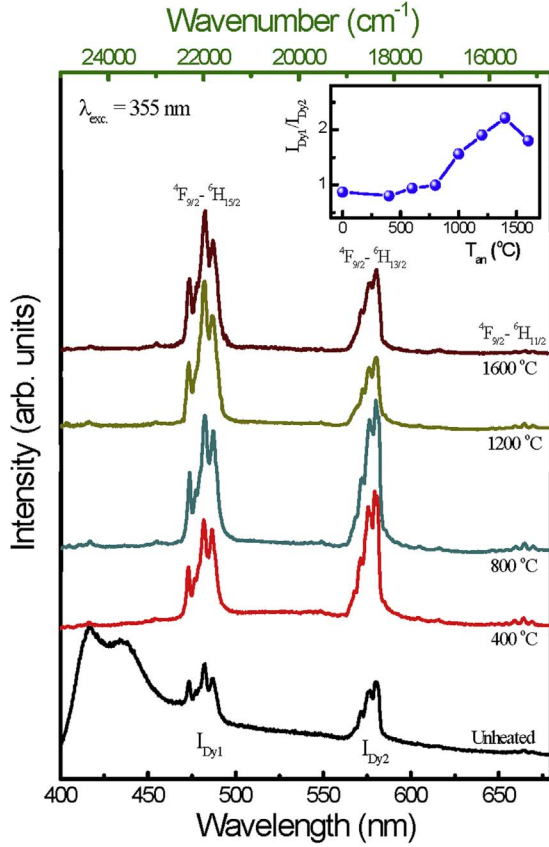


Fig. 8. PL spectra of some typical unheated and heated samples excited by wavelength $\lambda_{\text{exc}}=355$ nm. Sharp PL peaks are associated with electronic transitions ${}^4F_{9/2} \rightarrow ({}^6H_{15/2}, {}^6H_{13/2}, {}^6H_{11/2})$ of Dy^{3+} ions.

due to ${}^4F_{9/2} \rightarrow {}^6H_{15/2}$ and ${}^4F_{9/2} \rightarrow {}^6H_{13/2}$, respectively, the performance of the $I_{\text{Dy1}}/I_{\text{Dy2}}$ ratio versus indicate its dependence on T_{an} , the inset of Fig. 8. A significant change takes place as $T_{\text{an}} > 600$ °C is in good agreement with the variation tendencies of the unit-cell parameters, Fig. 3, and the $I_{\text{v}_3}/I_{\text{Tm}}$ and $I_{\text{v}_3}/I_{\text{Er}}$ ratios, Fig. 7(a). We think that the changes in I_{Dy1} and I_{Dy2} are related to not only the re-distribution and/or disappearance of defects and impurities versus high-temperature heat treatment, but also to crystal-field modifications surrounding Dy^{3+} ions. A slight decrease in $I_{\text{Dy1}}/I_{\text{Dy2}}$ for the $T_{\text{an}}=1600$ °C sample, the inset of Fig. 8, could be related to the gathering or evaporation of Dy^{3+} ions.

In good agreement with chemical-element analyses, the above RS and PL studies also demonstrated the presence of Dy^{3+} , Er^{3+} , Nd^{3+} and Tm^{3+} ions in the samples. The emissions associated with their electronic transitions persist with the samples, even for those annealed at high temperatures. Because the $T_{\text{an}}=1600$ °C sample is colorless and still indicates the persistence of all the RE ions, we thus believe that their electronic transitions are not responsible for initially reddish-brown color of natural zircons (i.e., the unheated sample) and pale reddish-brown samples.

As discussed above that the redistribution, clustering, and/or evaporation of defects and impurities would take place during heat treatment, changing the magnetic properties. In reference to this problem, we measured magnetic-field dependences of magnetization, $M(H)$ loops, of all the samples. Results shown in Fig. 9 demonstrate a coexistence of the paramagnetic (PM), and weak-ferromagnetic (FM) behaviors. These are certainly generated from defects and impurities (including both RE and transition-metal ions) because Zr^{4+} , Si^{4+} and O^{2-} ions in pure ZrSiO_4 are nonmagnetic. For the samples with $T_{\text{an}} < 1200$ °C, the PM phase associated with unpaired electrons (point defects) and isolated ions (known as PM centers) are dominant, leading

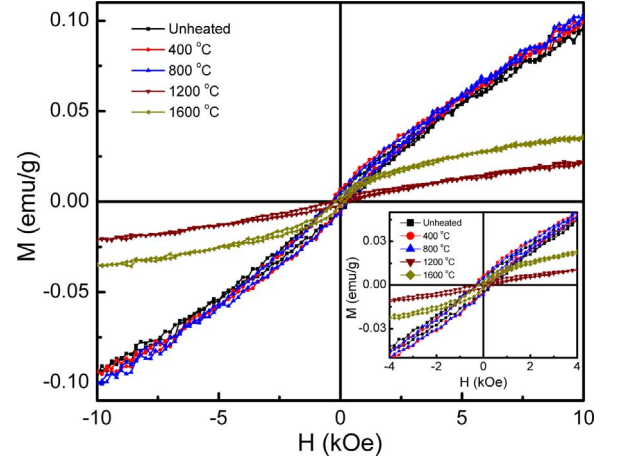


Fig. 9. Room-temperature hysteresis $M(H)$ loops of typical unheated and heated samples. The inset is an enlarged view of $M(H)$ data in the field range below 5 kOe.

to linear dependences of $M(H)$ at high fields. Meanwhile, FM contributions are weak, with saturation magnetization values $M_s=0.006\text{--}0.013$ emu/g and coercivity $H_c \approx 200$ Oe, which are mainly associated with exchange interactions between RE and/or transition-metal ions. The heat treatment in the range $T_{\text{an}}=1200\text{--}1400$ °C reduces strongly the PM signal (due to the reduction of point defects and isolated ions), without changing very much the FM ones. However, the annealing at higher temperatures, the cluttering of defects and impurities stimulates the coupling of their magnetic moments. This explains why FM order in the $T_{\text{an}}=1600$ °C sample slightly enhances, Fig. 9. In fact, the weak FM behavior was found in many mineral zircons [15], and their difference in magnetism is due to different concentrations of defects and impurities.

4. Conclusion

We studied the influence of heat treatment on the crystal structure, and optical and magnetic properties of natural reddish brown zircon. We found that its natural color became paled soon after the annealing at 400 °C, and colorless as $T_{\text{an}}=1600$ °C. The structural studies based on the XRD and RS techniques revealed that the annealing up to 1600 °C did not change in the $I41/amd$ tetragonal structure of the samples. However, there is a small modification of the unit-cell parameters, particularly for those with $T_{\text{an}} > 600$ °C, leading a remarkable change in relative intensity of the characteristic mode $\text{v}_3(\text{SiO}_4)$ of zircons at 1008 cm^{-1} . The PL study with different excitation wavelengths $\lambda_{\text{exc}}=355$, 532, and 785 nm also indicated the existence of RE ions of Dy^{3+} , Er^{3+} , Nd^{3+} , and Tm^{3+} . The PL emissions associated with their electronic transitions are narrow peaks and persist in all the samples. The consideration of the $I_{\text{v}_3}/I_{\text{Tm}}$, $I_{\text{v}_3}/I_{\text{Er}}$ and $I_{\text{Dy1}}/I_{\text{Dy2}}$ ratios revealed a strong dependence of PL intensities of RE ions on the annealing temperature T_{an} , which could be used to assess small structural changes taken place in natural zircon. Interestingly, the use of an excitation wavelength $\lambda_{\text{exc}}=355$ nm indicated stimulates broad PL emissions below 460 nm in the unheated sample, which are due to intrinsic defects. However, these emissions are completely absent in all the heated samples. The study of the magnetic properties revealed the coexistence of PM and weak-FM phases in the samples. Among these, the PM phase is due to unpaired electrons and isolated ions while the FM phase is mainly associated with exchange interactions between RE and/or transition-metal ions. The heat treatment above 1200 °C mainly affects PM signals, without changing very much the FM ones. Comparing with other samples, FM order in the $T_{\text{an}}=1600$ °C sample is highest. The results obtained from the analyses of the crystal structure, and optical and magnetic properties are in good accordance with each other.

Acknowledgments

This research were supported by a project funded by Vietnam National Foundation for Science and Technology Development (NAFOSTED) under grant number 105.01-2012.01.

References

- [1] A.A. Kaminskii, P. Becker, H. Rhee, O. Lux, H.J. Eichler, R. Kleinschrodt, R. Rückamp, H. Yoneda, A. Shirakawa, L. Bohatý, *Phys. Status Solidi B* 252 (2015) 305.
- [2] G.M. Herrera-Pérez, *Mater. Res.* 18 (2015) 1313.
- [3] R. Titorenkova, B. Mihailova, L. Konstantinov, *Can. Mineral.* 44 (2006) 1357.
- [4] B.A. Kolesov, C.A. Geiger, T. Armbruster, *Eur. J. Miner.* 13 (2001) 939.
- [5] M. Zhang, E.K.H. Salje, I. Farnan, A. Graeme-Barber, P. Daniel, R.C. Ewing, A.M. Clark, H. Leroux, *J. Phys.: Condens. Matter* 12 (2000) 1915.
- [6] A.A. Finch, J. Garcia-Guinea, D.E. Hole, P.D. Townsend, J.M. Hanchar, *J. Phys. D: Appl. Phys.* 37 (2004) 2795.
- [7] A. Gucsik, M. Zhang, C. Koeberl, E.K.H. Salje, S.A.T. Redfern, J.M. Pruneda, *Mineral. Mag.* 68 (2004) 801.
- [8] T. Chen, X. Zhang, W. Jiang, J. Liu, W. Jiang, Z. Xie, *J. Eur. Cer. Soc.* 36 (2016) 1811.
- [9] A. Kaiser, M. Lobert, R. Telle, *J. Eur. Cer. Soc.* 28 (2008) 2199.
- [10] L. Nasdala, P.W. Reiners, J.I. Garver, A.K. Kennedy, R.A. Stern, E. Balan, R. Wirth, *Am. Mineral.* 89 (2004) 219.
- [11] P. Dawson, M.M. Hargreave, G.R. Wilkinson, *J. Phys. C., Solid State Phys.* 4 (1971) 240.
- [12] C. Lenz, L. Nasdala, D. Talla, C. Hauzenberger, R. Seitz, U. Kolitsch, 415 1, 2015.
- [13] A. Wittwer, L. Nasdala, B. Wanthanachaisaeng, N. Bunnag, R. Škoda, W.A. Balmer, G. Giester, M. Zeug, *Conference on Raman and Luminescence Spectroscopy in the Earth Sciences, Universitätszentrum Althanstraße, Vienna*, p. 115, 2013.
- [14] M. Gaft, R. Reisfeld, G. Panczer, *Modern Luminescence Spectroscopy of Minerals and Materials*, Springer Mineralogy, New York, 2015.
- [15] M. Sato, S. Yamamoto, Y. Yamamoto, Y. Okada, M. Ohno, H. Tsunakawa, S. Maruyama, *Earth, Planets Space* 67 (2015) 150.